



Generalized thermoelastic MGT model for a functionally graded heterogeneous unbounded medium containing a spherical hole

Ahmed E. Abouelregal^{1,2,a}

¹ Department of Mathematics, College of Science and Arts, Jouf University, Al-Qurayyat, Saudi Arabia

² Department of Mathematics, Faculty of Science, Mansoura University, Mansoura, Egypt

Received: 27 January 2022 / Accepted: 6 August 2022

© The Author(s), under exclusive licence to Società Italiana di Fisica and Springer-Verlag GmbH Germany, part of Springer Nature 2022

Abstract This paper is intended to examine thermomechanical interactions within a functionally graded unbounded non-homogeneous solid with a spherical hole in a unified way using the Moore–Gibson–Thompson thermoelasticity (MGTE) model. The material has an inhomogeneity with the distribution of material properties in the radial direction determined by a power-law distribution. For the radial stress and temperature problems, the boundary conditions have been applied. The Laplace transform integral has been applied to get the analytical expressions for the thermophysical fields. Tables and graphs are shown to compare the accuracy of the suggested theory with the findings of previous models. The studied field variables have been numerically calculated and carefully discussed due to the effects of heterogeneity and relaxation.

1 Introduction

Heterogeneous substances are those that have non-uniform physical properties. These materials are also known as non-homogeneous materials because they contain a variety of mineral elements. These materials are of great importance in the design of future intelligent mixtures due to their superior mechanical properties and have many wide applications in the fields of science, technology, and engineering. Functionally gradient materials (FGMs) are an interesting and modern type of material with thermal and elastic properties that vary gradually and continuously across surfaces, thus reducing thermal stress. As a result, they are really useful in nuclear, aviation, and space technology. Geophysics, magnetic storage, plasma physics, and structural components, as well as the measurement of thermal elasticity, are just a few of the areas in which they can be used.

Many attempts have been devoted to the production of resistant materials in extreme temperatures because they are needed for many engineering purposes, such as thermal barrier coatings and engine components. FGMs, for example, were first used in Japan in the late 1980s as one of these products. Their macroscopic material properties are often different, separating them from laminated composite materials, which have major interlinear stresses that cause harm due to sudden shifts in physical properties across layer interfaces. The advantageous constituent stages for the achievement of high efficacy combine FGMs and laminated composite structures. References [1–11] and a recent book by Hetnarski and Eslami [12] are worth mentioning for some recent studies on FGMs in thermoelastic models.

In order to solve the failure of the model that a mechanical reason has no influence on a region of temperature, Biot [13] developed the theory of coupled thermoelasticity. This encouraged non-classical theories to be proposed, which meant replacing the equivalent thermal conductivity equation and Fourier's law with more general equations. Moreover, each generalization of thermal conductivity leads to the formation of a generalized theory of thermal elasticity. As an example, Lord and Shulman [14] improved the Fourier law of heat transfer. This model gives a hyperbolic type with a limited rate of thermal wave spread. The Lord–Shulman theory is also known as the extended thermoelastic generalized model. Green and Lindsay [15] established the temperature-rate-dependent thermoelasticity (TRDTE) model later with the implementation of two theoretical thermal relaxation factors, although the Fourier law in this model remains unchanged. The theory is based on two theoretical parameters.

Green and Naghdi [16–18], which have been the focus of active research in recent decades, are making an alternative theoretical development on this topic. Green and Naghdi made sufficient basic changes to the constitutive equations in this development and suggested three different thermoelasticity models, marked as types I, II, and III, thermoelastic, covering a much more extensive type of heat conduction problem. Chandrasekharaiah's dual-phase delay (DPL) thermoelastic model [19] is also stated here. This theoretical approach is based on another heat transfer equation called Tzou's two-phase model [20]. In addition to the previous models, a number of prevailing thermal elasticity models have been proposed that are based on these theories, which have been generalized in many papers [21–25].

^a e-mail: ahabogal@gmail.com (corresponding author)

The GN-II model proposed by Green and Naghdi was found to be able to resolve the obvious shortcoming of the infinite spread of thermal waves in thermal elasticity in the classical model, while the results verified the corresponding results of the GN-III theory, which showed that this theory leads to a deficiency like the conventional Fourier law. To address this shortcoming, Quintanilla [26, 27], Abouelregal et al. [28], and Abouelregal and Sedighi [29] have introduced a modification of the GN-III model with the addition of a relaxation parameter. The generalized theory of thermal elasticity proposed by Quintanilla [26, 27] has been developed by describing the equation of thermal conductivity using the Moore–Gibson–Thompson (MGT) equation.

In recent decades, the MGT equation has been progressively included in a broad range of papers focused on interpretation and comprehension. Kaltenbacher et al. [30] considered the Moore–Gibson–Thompson equation, which can be derived, for example, as a linearization of a model for wave propagation in viscous thermally relaxing fluids. This third order in the time equation exhibits a range of dynamical behaviors for its solutions that are dependent on the physical parameters in the equation, even in the linear version. Quintanilla is also analyzing the stability and well-being of the solutions in this theory [26]. Conti et al. [31] built a thermoelastic model of the MGT type based on the temperature background, and an integral differential formula from the MGT equation was considered. In the MGT thermoelastic model, Pellicer and Quintanilla [32] have greatly deepened their understanding of the uniqueness and instability of some thermomechanical problems. The basis of the theory proposed by Quintanilla [26] was a third-order differential equation developed in the field of fluid mechanics. Since its inception, the number of specialized studies in the field of thermoelastic theory MGT has increased significantly [33–37].

This paper focuses on the generalized theory of thermoelasticity, including the Moore–Gibson–Thompson heat equation (MGTE). The modified MGTE theory of thermoelasticity is a new generalized formula of the Lord–Shulman (LS) theory and the Green–Naghdi theory of thermoelasticity, which includes the energy dissipation of the third type (GN-III). The MGTE heat transfer model that has been developed reduces special cases to those of the previous generalized thermoelastic models. The functionally classified non-homogeneous thermoelastic sphere cavity is examined to verify the predictability of the current model. Except for the three phase layers, the properties of composite materials differ considerably according to the power law in the cavity.

The basic equations are accurately solved by means of the Laplace transform method, and the Laplace inversion process is employed to obtain the time field results numerically. The various influences on the distribution of analytical expressions of thermal relaxation and heterogeneity indicators have been studied graphically and analytically. The findings acquired in this article were as good as the published studies in the literature on methodology. We thought that the findings of this research would be useful in attempting to understand the fundamental characteristics of this new heat transfer model.

2 Basic equations

The governing system of equations and the constitutive relationships in the context of the model of the MGTE of thermoelasticity for an anisotropic medium can be expressed in the following manner [26, 29]:

The modified MGTE heat equation [26]:

$$\left(1 + \tau_0 \frac{\partial}{\partial t}\right) \vec{q} = -K \vec{\nabla} \theta - K^* \vec{\nabla} \vartheta \tag{1}$$

The energy balance equation:

$$\rho C_e \frac{\partial \theta}{\partial t} + \beta_{ij} T_0 \frac{\partial}{\partial t} (\vec{\nabla} \cdot \vec{u}) = -\vec{\nabla} \cdot \vec{q} + \rho Q \tag{2}$$

The stress–strain relations:

$$\sigma_{ij} = C_{ijkl} e_{kl} - \beta_{ij} \theta. \tag{3}$$

The relation between the displacement and strain:

$$e_{ij} = \frac{1}{2} (u_{j,i} + u_{i,j}). \tag{4}$$

The equation of motion:

$$\sigma_{ij,j} + F_i = \rho \ddot{u}_i \tag{5}$$

In Eqs. (1)–(5), \vec{q} denotes the heat flow, $\theta = T - T_0$ is the temperature change, T indicates the absolute temperature, T_0 denotes the environment temperature, K is the thermal conductivity, σ_{ij} is the stress tensor, e_{ij} is the strain tensor, u_i are the displacements, C_E is the specific heat, $\beta_{ij} = C_{ijkl} \alpha_{kl}$, C_{ij} are isothermal elastic constants, α_{kl} is the thermal expansion tensor, Q is the heat supply, ρ is the density, \vec{u} is the displacement vector, and F_i are the body force components. Also, the scalar function ϑ called the thermal displacement fulfills $\dot{\vartheta} = \theta$, and $K^* > 0$ is a material constant characteristic of Green and Naghdi theories called thermal conductivity rate.

By differentiating Eqs. (1) and (2) with respect to time and then removing \vec{q} from Eqs. (1) and (2) and using $\dot{\vartheta} = \theta$, the modified heat transfer MGTE equation can be obtained as:

$$\left(1 + \tau_0 \frac{\partial}{\partial t}\right) \left[\frac{\partial}{\partial t} \left(\rho C_E \frac{\partial \theta}{\partial t} \right) + T_0 \frac{\partial^2}{\partial t^2} (\beta_{ij} e_{ij}) - \frac{\partial Q}{\partial t} \right] = \nabla \cdot (K \nabla \theta) + \nabla \cdot (K^* \nabla \theta). \tag{6}$$

We make the assumption that the material constants satisfy $\rho > 0$, $C_E > 0$, $\beta_{ij} > 0$, $K^* > 0$, $K > 0$, and $K - \tau_0 K^* > 0$.

In this new model, the system of fundamental equations is completely hyperbolic, and both the kinetic equations and the heat transfer equation are hyperbolic. The problem of the propagation velocity of infinite heat waves found in the classical models is thus solved.

3 Special cases

From the basic equations in the previous section, some previous thermoelastic theories can be deduced as distinct states as follows:

- The conventional thermoelastic theory (CTE) [13] when $\tau_0 = 0$ and $K^* = 0$. The heat equation will be in the form:

$$K \nabla^2 \theta = \rho C_e \frac{\partial \theta}{\partial t} + T_0 \frac{\partial}{\partial t} (\beta_{ij} e_{ij}) - \rho Q. \tag{7}$$

- The Lord–Shulman theory (LS) [14] when $\tau_0 > 0$ and $K^* = 0$. The heat equation will be:

$$K \nabla^2 \theta = \left(1 + \tau_0 \frac{\partial}{\partial t}\right) \left(\rho C_e \frac{\partial \theta}{\partial t} + T_0 \frac{\partial}{\partial t} (\beta_{ij} e_{ij}) - \rho Q \right). \tag{8}$$

- The Green and Naghdi heat conduction equation (GN-II) [16] can be achieved if $K^* > 0$, $\tau_0 = 0$, and $K = 0$ as:

$$K^* \nabla^2 \theta = \frac{\partial}{\partial t} \left(\rho C_E \frac{\partial \theta}{\partial t} \right) + T_0 \frac{\partial^2}{\partial t^2} (\beta_{ij} e_{ij}) - \frac{\partial Q}{\partial t} \tag{9}$$

- The Green and Naghdi third-type model (GN-III) [17] can be obtained when $\tau_0 = 0$ as:

$$K \nabla^2 \dot{\theta} + K^* \nabla^2 \theta = \frac{\partial}{\partial t} \left(\rho C_E \frac{\partial \theta}{\partial t} \right) + T_0 \frac{\partial^2}{\partial t^2} (\beta_{ij} e_{ij}) - \frac{\partial Q}{\partial t}. \tag{10}$$

4 Application

In this section, as an application of the novel theory, we will study the problem of an infinitely flexible, heterogeneous, orthotropic thermal solid with a spherical hole of radius a to validate the accuracy of the suggested model. We assume that the interactions are spherically symmetric and use spherical polar coordinates (r, ϑ, φ) with the cavity origin at the center. Hence, all the interactions considered are therefore dependent on the distance r and time t only. The analysis will display only the radial displacement component $u_r = u(r, t)$.

In spherical coordinates, the thermal stresses for an orthotropic solid will be [38, 39]:

$$\sigma_{rr} = C_{11} e_{rr} + C_{12} (e_{\vartheta\vartheta} + e_{\varphi\varphi}) - \beta_{11} \theta, \tag{11}$$

$$\sigma_{\varphi\varphi} = \sigma_{\vartheta\vartheta} = C_{12} e_{rr} + C_{22} e_{\vartheta\vartheta} + C_{23} e_{\varphi\varphi} - \beta_{22} \theta, \tag{12}$$

with

$$\beta_{11} = \alpha_1 C_{11} + 2\alpha_2 C_{12}, \beta_{22} = \alpha_1 C_{12} + \alpha_2 C_{22} + \alpha_2 C_{23}. \tag{13}$$

where the parameters α_1 and α_2 are the coefficients of thermal expansion. The equation of motion can be written as:

$$\frac{\partial \sigma_{rr}}{\partial r} + \frac{2}{r} (\sigma_{rr} - \sigma_{\varphi\varphi}) = \rho \frac{\partial^2 u}{\partial t^2}. \tag{14}$$

The non-vanishing strains are given by

$$e_{rr} = \frac{\partial u}{\partial r}, e_{\vartheta\vartheta} = e_{\varphi\varphi} = \frac{u}{r}, e_{r\vartheta} = e_{r\varphi} = e_{\vartheta\varphi} = 0. \tag{15}$$

The thermal stresses may be expressed as:

$$\sigma_{rr} = C_{11} \frac{\partial u}{\partial r} + C_{12} \frac{2u}{r} - \beta_{11} \theta, \tag{16}$$

$$\sigma_{\varphi\varphi} = C_{12} \frac{\partial u}{\partial r} + (C_{22} + C_{23}) \frac{u}{r} - \beta_{22} \theta. \tag{17}$$

The MGTE heat Eq. (6) can be expressed as:

$$\left(1 + \tau_0 \frac{\partial}{\partial t}\right) \left[\rho C_e \frac{\partial^2 \theta}{\partial t^2} + T_0 \frac{\partial^2}{\partial r^2} \left(\beta_{11} \frac{\partial u}{\partial r} + \beta_{22} \frac{2u}{r} \right) \right] = \nabla \cdot (K \nabla \theta) + \nabla \cdot (K^* \nabla \theta). \tag{18}$$

The heterogeneity of the material is considered by taking into account that thermal conductivity, elastic coefficients, and density are entered into some laws of power with the variance of the radial distance r . Assume that the physical properties of the FGMs of the cavity are different in the radial direction and are defined as [38, 39]

$$C_{ij} = c_{ij} r^\xi, \rho = \rho_0 r^\xi, K = K_0 r^\xi, K^* = K_0^* r^\xi. \tag{19}$$

The parameter ξ is the heterogeneity index that governs the distribution of component materials through disk geometry. For an orthotropic homogeneous thermal medium, $\xi = 0$ and ρ_0, K_0, K_0^* , and c_{ij} are nonzero constants.

By using the above quantities, the governing equations will be in the following forms:

$$\sigma_{rr} = r^\xi \left[c_{11} \frac{\partial u}{\partial r} + c_{12} \frac{2u}{r} - \beta_1 \theta \right], \tag{20}$$

$$\sigma_{\varphi\varphi} = r^\xi \left[c_{12} \frac{\partial u}{\partial r} + (c_{22} + c_{23}) \frac{u}{r} - \beta_2 \theta \right], \tag{21}$$

$$c_{11} \frac{\partial^2 u}{\partial r^2} + c_{11} \frac{\xi + 2}{r} \frac{\partial u}{\partial r} + 2[c_{12}(\xi + 1) - (c_{22} + c_{23})] \frac{u}{r^2} - \beta_1 \frac{\partial \theta}{\partial r} - [\beta_1(\xi + 2) - 2\beta_2] \frac{\theta}{r} = \rho_0 \frac{\partial^2 u}{\partial t^2}, \tag{22}$$

$$\left(1 + \tau_0 \frac{\partial}{\partial t}\right) \left[\rho_0 C_e \frac{\partial^2 \theta}{\partial t^2} + T_0 \frac{\partial^2}{\partial r^2} \left(\beta_1 \frac{\partial u}{\partial r} + \beta_2 \frac{2u}{r} \right) \right] = K_0 \frac{\partial}{\partial t} \left(\frac{\partial^2 \theta}{\partial r^2} + \frac{\xi + 2}{r} \frac{\partial \theta}{\partial r} \right) + K_0^* \left(\frac{\partial^2 \theta}{\partial r^2} + \frac{\xi + 2}{r} \frac{\partial \theta}{\partial r} \right), \tag{23}$$

where

$$\beta_1 = \alpha_1 c_{11} + 2\alpha_2 c_{12}, \beta_2 = \alpha_1 c_{12} + \alpha_2 (c_{22} + c_{23}) \tag{24}$$

To simplify the problem, we present the following dimensionless variables and symbols:

$$R = \frac{r}{a}, U = \frac{C_{11}}{\beta_1 a T_0} u, \{\tau, \tau_q\} = \frac{v}{a} \{t, \tau_0\}, \Theta = \frac{\theta}{T_0}, \tau_{ij} = \frac{\sigma_{ij}}{\beta_1 T_0}, v = \sqrt{\frac{C_{11}}{\rho}}. \tag{25}$$

In light of Eq. (25), the non-dimensional forms of Eqs. (20)–(23) can be simplified as follows:

$$\tau_{rr} = R^\xi \left[\frac{\partial U}{\partial R} + \lambda_1 \frac{2U}{R} - \Theta \right], \tag{26}$$

$$\tau_{\varphi\varphi} = R^\xi \left[\lambda_1 \frac{\partial U}{\partial R} + \lambda_2 \frac{U}{R} - \beta \Theta \right], \tag{27}$$

$$\left(1 + \tau_q \frac{\partial}{\partial \tau}\right) \left[\frac{\partial^2 \Theta}{\partial \tau^2} + \varepsilon \frac{\partial^2}{\partial R^2} \left(\frac{\partial U}{\partial R} + \beta \frac{2U}{R} \right) \right] = K_1 \frac{\partial}{\partial \tau} \left(\frac{\partial^2 \Theta}{\partial R^2} + \frac{\xi + 2}{R} \frac{\partial \Theta}{\partial R} \right) + K_2 \left(\frac{\partial^2 \Theta}{\partial R^2} + \frac{\xi + 2}{R} \frac{\partial \Theta}{\partial R} \right), \tag{28}$$

$$\frac{\partial^2 U}{\partial R^2} + \frac{\xi + 2}{R} \frac{\partial U}{\partial R} - m \frac{U}{R^2} - \frac{\partial^2 u}{\partial \tau^2} = \frac{\partial \Theta}{\partial R} + h \frac{\Theta}{R}, \tag{29}$$

where

$$\lambda_1 = \frac{c_{12}}{c_{11}}, \lambda_2 = \frac{c_{22} + c_{23}}{c_{11}}, \beta = \frac{\beta_2}{\beta_1}, K_1 = \frac{K_0}{av\rho_0 C_e}, K_2 = \frac{K_0^*}{v^2 \rho_0 C_e}, \tag{30}$$

$$\varepsilon = \frac{T_0 \beta_1^2}{c_{11} \rho_0 C_e}, m = 2[\lambda_2 - \lambda_1(\xi + 1)], h = (\xi + 2) - 2\beta.$$

To determine the boundary conditions of the problem, we shall consider the surface of the spherical socket to be free of traction but subject to thermal shock. As a result, the thermophysical boundary conditions at the cavity’s internal surface are described as:

$$\begin{aligned} \tau_{rr}(R, \tau) &= 0 \text{ at } R = 1, t > 0, \\ \Theta(R, \tau) &= \Theta_1 H(\tau), \text{ at } R = 1, t > 0, \end{aligned} \tag{31}$$

where Θ_1 is the positive constant and $H(t)$ is the Heaviside function.

5 Transformed solution

The Laplace transform method is applied to Eqs. (26) to (29), under the following initial conditions:

$$\begin{aligned}
 U(R, \tau) = 0, \frac{\partial U(R, \tau)}{\partial R} = 0, \frac{\partial^2 U(R, \tau)}{\partial \tau^2} = 0, \text{ at } \tau = 0, \\
 \Theta(R, \tau) = 0, \frac{\partial \Theta(R, \tau)}{\partial R} = 0, \frac{\partial^2 \Theta(R, \tau)}{\partial \tau^2} = 0 \text{ at } \tau = 0.
 \end{aligned}
 \tag{32}$$

Then, the transformed equations can be expressed as:

$$\bar{\tau}_{rr} = R^\xi \left[\frac{d\bar{U}}{dR} + \lambda_1 \frac{2\bar{U}}{R} - \bar{\Theta} \right]
 \tag{33}$$

$$\bar{\tau}_{\varphi\varphi} = R^\xi \left[\lambda_1 \frac{d\bar{U}}{dR} + \lambda_2 \frac{\bar{U}}{R} - \beta \bar{\Theta} \right],
 \tag{34}$$

$$\left[s^2 \bar{\Theta} + \varepsilon s^2 \left(\frac{d\bar{U}}{dR} + \frac{\xi + 2}{R} \bar{U} \right) \right] = \lambda_3 \left(\frac{d^2 \bar{\Theta}}{dR^2} + \frac{\xi + 2}{R} \frac{d\bar{\Theta}}{dR} \right),
 \tag{35}$$

$$\frac{d^2 \bar{U}}{dR^2} + \frac{\xi + 2}{R} \frac{d\bar{U}}{dR} - \frac{\xi + 2}{R} \frac{\bar{U}}{R} - s^2 \bar{U} = \frac{d\bar{\Theta}}{dR}
 \tag{36}$$

where we assume that $\beta = (\xi + 2)/2$, $m = (\xi + 2)$, and $\lambda_3 = \frac{K_1 s + K_2}{1 + \tau_0 s}$.

We are now going to introduce a new function ψ described by the relation:

$$\bar{U} = \frac{d\bar{\Psi}}{dR}
 \tag{37}$$

Then, Eqs. (35) and (36) can be rewritten in the form:

$$(D_1 D_2 - s^2) \bar{\Psi} = \bar{\Theta}
 \tag{38}$$

$$\varepsilon s^2 D_1 D_2 \bar{\Psi} = \lambda_3 (D_1 D_2 - s^2) \bar{\Theta}
 \tag{39}$$

where

$$D_1 = \frac{d}{dR} + \frac{\xi + 2}{R}, D_2 = \frac{d}{dR}.
 \tag{40}$$

From Eqs. (38), and (39), we can obtain:

$$(D_1 D_2 - m_1^2)(D_1 D_2 - m_2^2) \bar{\Psi} = 0,
 \tag{41}$$

where m_1^2 and m_2^2 satisfy the equation:

$$m^4 - \left[2s^2 + \frac{\varepsilon s^2}{\lambda_3} \right] m^2 + s^4 = 0.
 \tag{42}$$

A new dependent function $\bar{\Phi}$ is presented to convert Eq. (41) into a modified Bessel equation:

$$\bar{\Phi} = R^{-\nu} \bar{\Psi}, \nu = (\xi + 1)/2.
 \tag{43}$$

Then, Eq. (41) can be rewritten in the following form:

$$\left(\frac{d^2}{dR^2} + \frac{1}{R} \frac{d}{dR} - \left(\frac{\nu^2}{R^2} + m_1^2 \right) \right) \left(\frac{d^2}{dR^2} + \frac{1}{R} \frac{d}{dR} - \left(\frac{\nu^2}{R^2} + m_2^2 \right) \right) \bar{\Phi} = 0.
 \tag{44}$$

The general solution to the function $\bar{\Psi}$ can be found in the form:

$$\bar{\Psi} = R^\nu \sum_{i=1}^2 [A_i K_\nu(m_i R) + B_i I_\nu(m_i R)],
 \tag{45}$$

where the functions $I_\nu(\cdot)$ and $K_\nu(\cdot)$ denote the modified Bessel functions of the first and second kinds, respectively. The parameters A_i, B_i ($i = 1, 2$) are integral coefficients. For the solution to be continuous everywhere within the spherical cavity of the body and for the uniformity condition, we take the parameters $B_i = 0$.

It follows from Eqs. (37) and (45) that

$$\bar{U} = -R^\nu \sum_{i=1}^2 A_i m_i K_{\nu-1}(m_i R). \tag{46}$$

The expression of the temperature $\bar{\Theta}$ may be achieved by substituting Eq. (45) into Eq. (38) as:

$$\bar{\Theta} = R^\nu \sum_{i=1}^2 A_i \left[(m_i^2 - s^2) K_{\nu-2}(m_i R) - \frac{2s^2(\nu - 1) + m_i^2(\nu + 3)}{m_i R} K_{\nu-1}(m_i R) \right]. \tag{47}$$

Substituting the functions \bar{U} and $\bar{\Theta}$ into Eqs. (33) and (34), we obtain the stress components as:

$$\bar{\tau}_{rr} = R^{2\nu} \sum_{i=1}^2 \frac{A_i}{m_i} \left[m_i s^2 K_{\nu-2}(m_i R) + \frac{m_i^2(\nu + 2 + 2\lambda_1) + 2s^2(\nu - 1)}{m_i R} K_{\nu+1}(m_i R) \right], \tag{48}$$

$$\bar{\tau}_{\varphi\varphi} = R^{2\nu} \sum_{i=1}^2 \frac{A_i}{m_i} \left((m_i \beta s^2 + m_i^3(\lambda_1 - \beta)) K_{\nu-2}(m_i R) + \frac{m_i^2(\nu + 3) - m_i^2(\lambda_1 + \lambda_2) + 2\beta s^2(\nu - 1)}{m_i R} K_{\nu+1}(m_i R) \right), \tag{49}$$

The boundary conditions (31) after performing the Laplace transform method are as follows:

$$\begin{aligned} \bar{\tau}_{rr}(R, s) &= 0 \text{ at } R = 1, \\ \bar{\Theta}(R, s) &= \frac{\Theta_1}{s}, \text{ at } R = 1. \end{aligned} \tag{50}$$

When the solutions in Eqs. (47) and (48) are substituted in terms of the aforementioned boundary conditions, we get:

$$\sum_{i=1}^2 \frac{A_i}{m_i} \left[m_i s^2 K_{\nu-2}(m_i) + \frac{m_i^2(\nu + 2 + 2\lambda_1) + 2s^2(\nu - 1)}{m_i} K_{\nu+1}(m_i) \right] = 0, \tag{51}$$

$$\sum_{i=1}^2 A_i \left[(m_i^2 - s^2) K_{\nu-2}(m_i) - \frac{2s^2(\nu - 1) + m_i^2(\nu + 3)}{m_i} K_{\nu-1}(m_i) \right] = \frac{\Theta_1}{s}. \tag{52}$$

We can obtain the integration constants A_i , ($i = 1, 2$) by solving Eqs. (51) and (52).

Once the integration constants have been determined, we have the solutions for all areas studied in the field of Laplace transform. An accurate, effective, and well-proven numerical technique based on the expansion of the Fourier series [40] will be used to find Laplace’s inverse transformations. The following methodology can be used to represent any function in the Laplace domain in the time domain:

$$g(R, \tau) = \frac{e^{\omega\tau}}{\tau} \left(\frac{1}{2} \bar{g}(R, \omega) + Re \sum_{n=1}^k \bar{g} \left(R, \omega + \frac{in\pi}{\tau} \right) (-1)^n \right), \tag{53}$$

where k represents a finite number of terms and the value of ω satisfies the relation $\omega\tau \cong 4.7$ for faster convergence [40].

6 Results and Discussion

In this section, the numerical results of the theoretical solutions obtained in the previous section are found numerically using the algorithm (53) to study and investigate the proposed model. Using the Mathematica programming language, the numerical code has been developed. For the purpose of numerical calculations, the following values will be taken into account:

$$\begin{aligned} c_{11} &= 5.974 \times 10^{10} \frac{\text{N}}{\text{m}^2}, c_{12} = 2.624 \times 10^{10} \frac{\text{N}}{\text{m}^2}, \Theta_1 = 0.5, \rho_0 = 1470 \frac{\text{kg}}{\text{m}^3}, \\ c_{23} &= 2.17 \times 10^{10} \frac{\text{N}}{\text{m}^2}, c_{33} = 6.17 \times 10^{10} \frac{\text{N}}{\text{m}^2}, K_0^* = 200 \frac{\text{W}}{\text{s m K}}, \varepsilon = 0.0202, \\ C_E &= 140 \frac{\text{J}}{\text{kg K}}, T_0 = 298\text{K}, \beta_1 = \beta_2 = 2.68 \times 10^6 \frac{\text{N}}{\text{m}^2 \text{K}}, K_0 = 386, \end{aligned}$$

$$C_E = 140 \frac{\text{J}}{\text{kg K}}, T_0 = 298\text{K}, \beta_1 = \beta_2 = 2.68 \times 10^6 \frac{\text{N}}{\text{m}^2 \text{K}}, K_0 = 386 \frac{\text{W}}{\text{m K}}.$$

Some numerical calculations were made for a single value of time t , that is, $t = 0.12$ if not stated otherwise. The profiles of the thermodynamic temperature Θ , displacement U , and thermal stresses τ_{rr} and $\tau_{\varphi\varphi}$ with various locations of R are determined numerically. It is helpful to summarize the data in tabular form in this section in order to demonstrate the comparison between the various thermoelasticity models. Our findings will also be tabulated in tabular form to assist other investigators in evaluating and

Fig. 1 The variation of the temperature Θ for heterogeneity index ξ

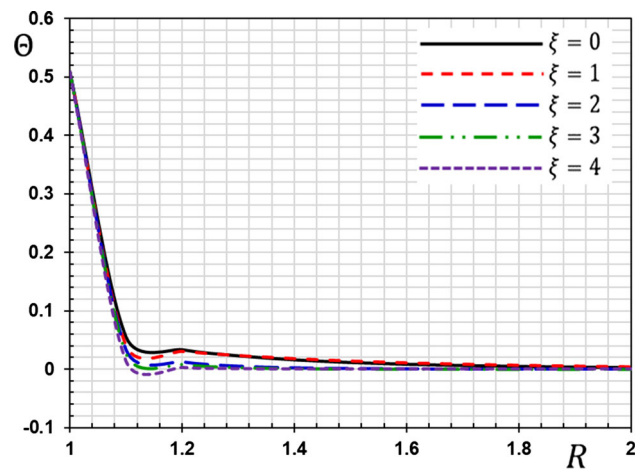
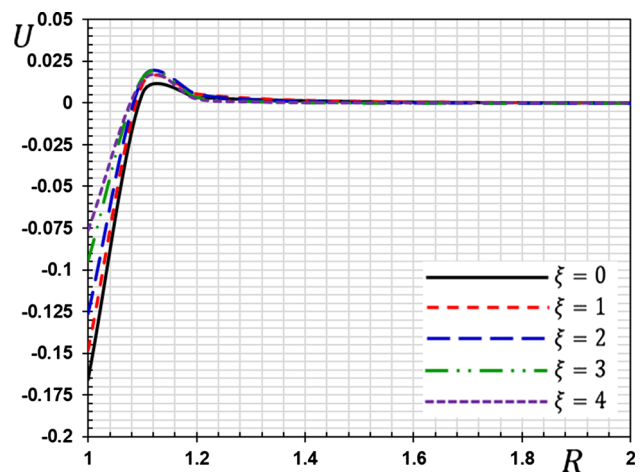


Fig. 2 The variation of the displacement U for heterogeneity index ξ



validating their findings. A thermoelastic medium comparative study has been carried out, and time and heterogeneity index effects have been analyzed.

Theoretical research in the field of functionally graded (FG) structures has become essential for continuum mechanics as a result of the widespread use of high-temperature substances in industrial technology and the use of biology and geology in materials science. The spread of heat waves in elastic materials is important in a variety of fields, including seismic analysis, soil mechanics, nuclear reactors, high-energy particle accelerators, and more. It was illustrated that governed gradients with mechanical properties provide the possibility of designing contact deformation and damage-resistant surfaces, which cannot be done in conventional uniform materials.

The purpose of this report was to explain the effect of the non-homogeneity index of the FG material on the thermophysical fields. Figures 1, 2, 3, 4 and Tables 1, 2, 3, 4 present variants of the dimensional, thermodynamic temperature, and thermal stresses in the radial direction of the FG spherical hole. The figures and tables display the numerical results in detail for various situations. Computation has been done for a wide range of non-homogeneity index ξ values, via $\xi = 1, 2, 3, 4$. We can also compare and contrast homogeneous and non-homogeneous cases. In addition, $\xi = 0$ leads to a homogeneous case. In this case, the study and discussion will take place in the context of the modified MGTE theory.

The temperature variation Θ versus radius variable R for various non-homogeneity indices is presented in Fig. 1 and Table 1. Table 1 illustrates that the temperature change Θ at the cavity surface ($R = 1$) is greater, satisfying the conditions for the thermal limit, and then declines with a progressive increase in R -radius. In all cases, the temperature values tend to be zero, with the radius increasing asymptotically. The non-homogeneity parameter has a noticeable impact on temperature behavior. The increase in the classified parameter reduces thermal wave speed and temporary minimum temperature. In addition, the case for homogeneous materials is caused by $\xi = 0$. In Fig. 1, the rate of temperature decline Θ was observed to be faster for $\xi = 4$ than for $\xi = 1, 2, 3$.

For various values of the parameter ξ , Fig. 2 and Table 2 give the variance of the observation displacement U with distance R . The displacement U appears to take negative values and increases gradually until it reaches a peak value in a certain location close to the surface of the cavity and then decreases rapidly inside the medium with a greater distance R . It has been discovered that FGM has a significant impact on displacement variation. By increasing the parameters of the graded index, the values of the displacement increase. Furthermore, its magnitude decreases as R increases, which is physically possible.

Fig. 3 The variation of the radial stress τ_{rr} for heterogeneity index ξ

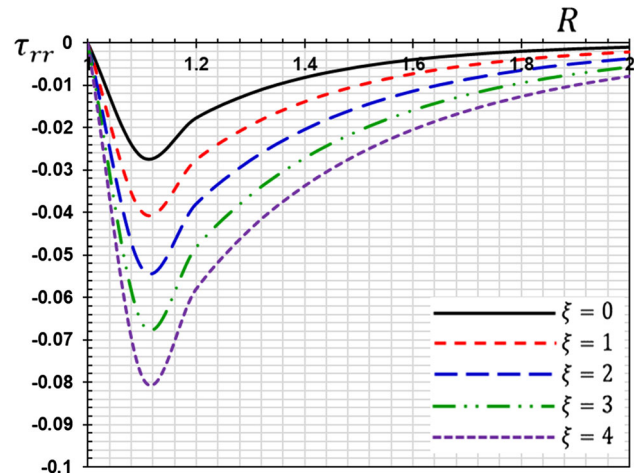


Fig. 4 The variation of the hoop stress $\tau_{\phi\phi}$ for heterogeneity index ξ

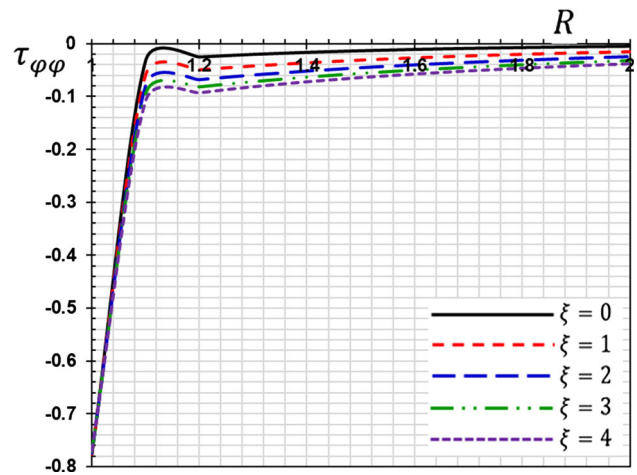


Table 1 The variation of the temperature Θ for heterogeneity index ξ

| R | $\xi = 0$ | $\xi = 1$ | $\xi = 2$ | $\xi = 3$ | $\xi = 4$ |
|-----|-----------|-----------|-----------|-----------|-----------|
| 1.0 | 0.50914 | 0.50914 | 0.50914 | 0.50914 | 0.50914 |
| 1.1 | 0.055157 | 0.041441 | 0.0334843 | 0.02697 | 0.01339 |
| 1.2 | 0.033037 | 0.031169 | 0.0124836 | 0.00847 | 0.002497 |
| 1.3 | 0.022505 | 0.024011 | 0.0050618 | 0.002937 | 0.000539 |
| 1.4 | 0.015658 | 0.018689 | 0.0021873 | 0.001099 | 0.00013 |
| 1.5 | 0.011092 | 0.014676 | 0.0009983 | 0.000439 | 3.46E-05 |
| 1.6 | 0.007981 | 0.011614 | 0.0004777 | 0.000185 | 1E-05 |
| 1.7 | 0.005821 | 0.009253 | 0.0002383 | 8.23E-05 | 3.11E-06 |
| 1.8 | 0.004296 | 0.007415 | 0.0001233 | 3.82E-05 | 1.03E-06 |
| 1.9 | 0.003205 | 0.005974 | 6.591E-05 | 1.84E-05 | 3.63E-07 |
| 2.0 | 0.002413 | 0.004835 | 3.627E-05 | 9.19E-06 | 1.35E-07 |

Figures 3 and 4 show the radial and hoop stresses τ_{rr} and $\tau_{\phi\phi}$ with the same constant value as the graded parameter to show the effect of the non-homogeneous material index ξ . In addition, they show the difference between homogenous and non-homogenous materials in the two cases. In the bounding plane $R = 1$, the radial stress τ_{rr} disappears, and the mechanical boundary condition is met. The radial stress τ_{rr} increases with the graded material index ξ . The values of the stress increase with R to reach their minimum point at $R = 1.1$ with different values of the graded material index. It then declines slightly to zero at the medium points. Figure 4 depicts the hoop stresses $\tau_{\phi\phi}$ distribution of the FGM unbounded solid with a spherical hole versus the radial direction R for various values of ξ . It can be shown that the stress $\tau_{\phi\phi}$ rises sharply within a narrow range of radial direction at first, then steadily increases to its maximum value, and then decreases as R increases. The stress $\tau_{\phi\phi}$ decreases with the increase in graded material index ξ . The

Table 2 The variation of the displacement U for heterogeneity index ξ

| R | $\xi = 0$ | $\xi = 1$ | $\xi = 2$ | $\xi = 3$ | $\xi = 4$ |
|-----|-----------|-----------|-----------|-----------|-----------|
| 1.0 | -0.16577 | -0.14838 | -0.12655 | -0.09439 | -0.07662 |
| 1.1 | 0.005587 | 0.011132 | 0.01474 | 0.015015 | 0.013099 |
| 1.2 | 0.003493 | 0.005401 | 0.005419 | 0.003562 | 0.002305 |
| 1.3 | 0.002256 | 0.002818 | 0.002234 | 0.001010 | 0.000506 |
| 1.4 | 0.001494 | 0.001552 | 0.001004 | 0.000328 | 0.000131 |
| 1.5 | 0.001008 | 0.000891 | 0.000482 | 0.000118 | 3.88E-05 |
| 1.6 | 0.000690 | 0.000529 | 0.000244 | 4.64E-05 | 1.28E-05 |
| 1.7 | 0.000478 | 0.000323 | 0.000129 | 1.95E-05 | 4.57E-06 |
| 1.8 | 0.000335 | 0.000201 | 7.10E-05 | 8.69E-06 | 1.76E-06 |
| 1.9 | 0.000236 | 0.000128 | 4.01E-05 | 4.06E-06 | 7.18E-07 |
| 2.0 | 0.000168 | 8.25E-05 | 2.33E-05 | 1.98E-06 | 3.09E-07 |

Table 3 The variation of the radial stress τ_{rr} for heterogeneity index ξ

| R | $\xi = 0$ | $\xi = 1$ | $\xi = 2$ | $\xi = 3$ | $\xi = 4$ |
|-----|-----------|-----------|-----------|-----------|-----------|
| 1.0 | 0 | 0 | 0 | 0 | 0 |
| 1.1 | -0.02685 | -0.03983 | -0.053 | -0.06594 | -0.07846 |
| 1.2 | -0.01772 | -0.0276 | -0.03798 | -0.04824 | -0.05801 |
| 1.3 | -0.01195 | -0.01947 | -0.0277 | -0.036 | -0.04393 |
| 1.4 | -0.00819 | -0.01392 | -0.02045 | -0.02722 | -0.03377 |
| 1.5 | -0.00569 | -0.01005 | -0.01523 | -0.02076 | -0.02622 |
| 1.6 | -0.00399 | -0.00731 | -0.01142 | -0.01593 | -0.02049 |
| 1.7 | -0.00282 | -0.00535 | -0.0086 | -0.01228 | -0.01608 |
| 1.8 | -0.00201 | -0.00394 | -0.0065 | -0.00949 | -0.01266 |
| 1.9 | -0.00144 | -0.00291 | -0.00493 | -0.00735 | -0.00999 |
| 2.0 | -0.00104 | -0.00216 | -0.00374 | -0.00571 | -0.00789 |

Table 4 The variation of the hoop stress $\tau_{\varphi\varphi}$ for heterogeneity index ξ

| R | $\xi = 0$ | $\xi = 1$ | $\xi = 2$ | $\xi = 3$ | $\xi = 4$ |
|-----|-----------|-----------|-----------|-----------|-----------|
| 1.0 | -0.77836 | -0.77666 | -0.77453 | -0.77237 | -0.77047 |
| 1.1 | -0.03233 | -0.05801 | -0.07893 | -0.09498 | -0.10775 |
| 1.2 | -0.02585 | -0.04890 | -0.06804 | -0.08233 | -0.09309 |
| 1.3 | -0.02100 | -0.04163 | -0.05924 | -0.07222 | -0.08160 |
| 1.4 | -0.01715 | -0.03558 | -0.05182 | -0.06376 | -0.07213 |
| 1.5 | -0.01408 | -0.03051 | -0.04549 | -0.05656 | -0.06419 |
| 1.6 | -0.01161 | -0.02623 | -0.04004 | -0.05038 | -0.05742 |
| 1.7 | -0.00961 | -0.02260 | -0.03533 | -0.04501 | -0.05159 |
| 1.8 | -0.00798 | -0.01951 | -0.03123 | -0.04032 | -0.04651 |
| 1.9 | -0.00665 | -0.01687 | -0.02765 | -0.03618 | -0.04204 |
| 2.0 | -0.00555 | -0.01461 | -0.02451 | -0.03252 | -0.03809 |

material scaling concept for engineers and technicians is an effective tool for designing new materials for some special applications such as aerospace, automotive, biomedicine, nuclear power, and gas turbine engines.

The thermoelastic MGTE model is a widespread form of both the Lord–Shulman (LS) model and the thermoelastic theory of Green–Naghdi (GN). Thermophysical field quantities vary according to the radial distance variable R for the classical model (CTE), the generalized LS, GN-II, GN-III models, and the introduced model MGTE, as shown in Figs. 5, 6, 7, and 8 and Tables 5, 6, 7, and 8. Here, the parameter $\xi = 2$ is considered for the non-homogeneity index.

Figure 5 and Table 5 show the thermodynamic temperature Θ variation compared with R for different thermoelasticity models. The maximum temperature values for the GN-III models are observed. For all models, the temperature magnitude approaches zero asymptotically, with R growing. Moreover, as illustrated in Fig. 5 and Table 5, the thermal wave speed of both CTE and GN-III is greater than that of the LS, GN-II, and MGTE models. The variation in the displacement U in the FG hollow sphere is described in Fig. 6 and Table 6. There are very clear differences between the CTE, LS, GN-II, GN-III, and MGTE models. The thermal

Fig. 5 The temperature Θ for different models of thermoelasticity

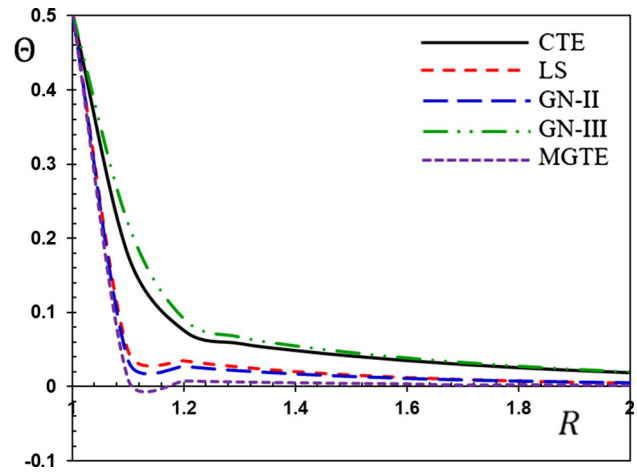


Fig. 6 The displacement U for different models of thermoelasticity

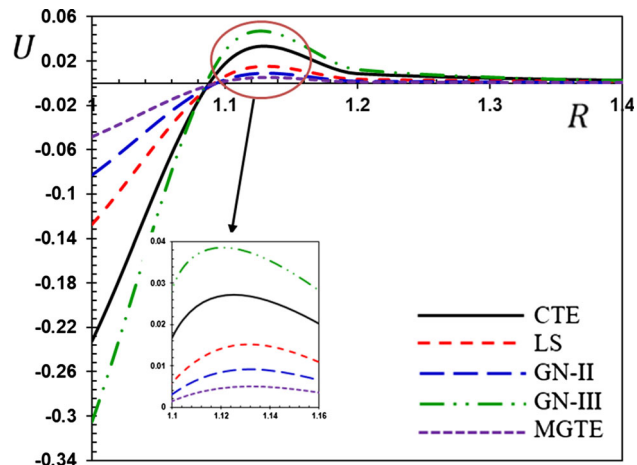
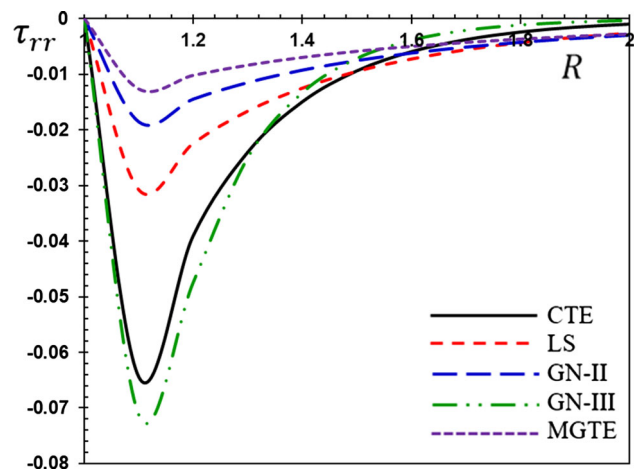


Fig. 7 The radial thermal stress τ_{rr} for different models of thermoelasticity



parameters τ_q , K_0 , and K_0^* all have a significant impact on the displacement distribution. The difference between the results in CTE, LS, GN-II, GN-III, and MGTE is very clear. All five models have been found to yield nearly the same number of results. This also ensures that our numerical results are checked properly.

Table 7 and Fig. 7 illustrate the changes in the radial stress τ_{rr} over the radial cavity direction R . In comparison with those based on different models, we demonstrate the validity of radial stress τ_{rr} according to the MGTE model. The table shows that the pressure τ_{rr} vanishes to satisfy the physical boundary condition on the surface of the cavity. In addition, the highest point for CTE and CN-III models is the amplitude of the radial thermal stress τ_{rr} . In addition, the magnitude of thermal stress decreases slightly as we move away from the cavity surface in all five models. In addition, for the GN-III model, the radial stress τ_{rr} profile is bigger than the

Fig. 8 The variation of the hoop stress $\tau_{\varphi\varphi}$ for different models of thermoelasticity

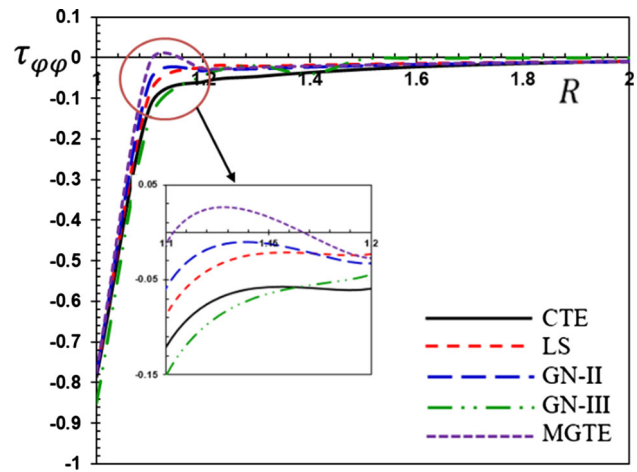


Table 5 The variation of the temperature Θ for different models of thermoelasticity

| R | CTE | LS | GN-II | GN-III | MGTE |
|-----|-----------|-----------|-----------|-----------|-----------|
| 1.0 | 0.5035914 | 0.5035914 | 0.5035914 | 0.5035914 | 0.5035914 |
| 1.1 | 0.176532 | 0.0475944 | 0.0348478 | 0.219216 | 0.0099032 |
| 1.2 | 0.0755568 | 0.0349325 | 0.0268172 | 0.0909881 | 0.0081571 |
| 1.3 | 0.058138 | 0.0265408 | 0.0209852 | 0.0665647 | 0.0068085 |
| 1.4 | 0.0487149 | 0.0203734 | 0.016594 | 0.054645 | 0.0057472 |
| 1.5 | 0.0412602 | 0.0157773 | 0.0132398 | 0.0456591 | 0.0048984 |
| 1.6 | 0.0350657 | 0.0123114 | 0.0106459 | 0.0383225 | 0.00421 |
| 1.7 | 0.0298777 | 0.0096711 | 0.0086184 | 0.0322516 | 0.002645 |
| 1.8 | 0.0255162 | 0.0076418 | 0.007019 | 0.0272053 | 0.0031763 |
| 1.9 | 0.0218381 | 0.0060698 | 0.0057468 | 0.0229974 | 0.0027839 |
| 2.0 | 0.0187275 | 0.0048438 | 0.0047275 | 0.0194788 | 0.0024525 |

Table 6 The displacement U for different models of thermoelasticity

| R | CTE | LS | GN-II | GN-III | MGTE |
|-----|------------|------------|-------------|------------|-------------|
| 1.0 | - 0.232655 | - 0.127566 | - 0.0828299 | - 0.305301 | - 0.0485819 |
| 1.1 | 0.0168928 | 0.0059602 | 0.0031146 | 0.0288585 | 0.0015273 |
| 1.2 | 0.0083267 | 0.0034268 | 0.0018786 | 0.0124536 | 0.0009462 |
| 1.3 | 0.0043039 | 0.0020797 | 0.0011999 | 0.0055802 | 0.0006223 |
| 1.4 | 0.0023053 | 0.0013143 | 0.0008002 | 0.0025851 | 0.0004283 |
| 1.5 | 0.0012692 | 0.0008569 | 0.0005519 | 0.0012287 | 0.0003054 |
| 1.6 | 0.0007141 | 0.0005728 | 0.0003909 | 0.000596 | 0.0002241 |
| 1.7 | 0.0004089 | 0.0003906 | 0.000283 | 0.0002939 | 0.0001683 |
| 1.8 | 0.0002376 | 0.0002708 | 0.0002086 | 0.0001469 | 0.0001288 |
| 1.9 | 0.0001397 | 0.0001904 | 0.0001561 | 7.427E-05 | 0.0001003 |
| 2.0 | 8.301E-05 | 0.0001355 | 0.0001183 | 3.792E-05 | 7.912E-05 |

thermoelastic LS and GN-III designs, which is again larger than the MGTE model. Finally, it is worth noting that the relaxation parameter plays an important role in the progression of radial thermal stress.

Table 8 and Fig. 8 show the influences of various thermoelasticity values on the hoop stress distribution $\tau_{\varphi\varphi}$ of the medium for various thermoelasticity models when $\xi = 2$. The values for the distribution of hoop stress $\tau_{\varphi\varphi}$ across the cavity range are given in Table 4. For various thermoelastic models, the same behavior occurs. The table shows that the size of the hoop stress $\tau_{\varphi\varphi}$ rises and then achieves zero values, with the R gap for the different models increasing. Furthermore, it has been noticed that relaxation time has a significant impact on the hoop stress $\tau_{\varphi\varphi}$. Depending on the values of thermal parameters, the thermal waves reach a constant state.

Table 7 The radial thermal stress τ_{rr} for different models of thermoelasticity

| R | CTE | LS | GN-II | GN-III | MGTE |
|-----|------------|------------|------------|------------|------------|
| 1.0 | 0 | 0 | 0 | 0 | 0 |
| 1.1 | -0.0643996 | -0.0307859 | -0.0185261 | -0.0712179 | -0.0126388 |
| 1.2 | -0.038963 | -0.0224193 | -0.014434 | -0.0473525 | -0.0101693 |
| 1.3 | -0.0239833 | -0.0166338 | -0.0114702 | -0.0249695 | -0.0083524 |
| 1.4 | -0.014948 | -0.0125089 | -0.0092466 | -0.013328 | -0.0069636 |
| 1.5 | -0.0094046 | -0.0095033 | -0.0075354 | -0.0071797 | -0.0058723 |
| 1.6 | -0.0059605 | -0.0072774 | -0.0061934 | -0.0038955 | -0.0049964 |
| 1.7 | -0.0037999 | -0.0056085 | -0.0051251 | -0.0021257 | -0.0042818 |
| 1.8 | -0.0024342 | -0.0043449 | -0.0042649 | -0.0011654 | -0.0036911 |
| 1.9 | -0.0015656 | -0.0033806 | -0.0035656 | -0.0006414 | -0.0031975 |
| 2.0 | -0.0010103 | -0.00264 | -0.0029927 | -0.0003542 | -0.0027815 |

Table 8 The hoop stress $\tau_{\varphi\varphi}$ for different models of thermoelasticity

| R | CTE | LS | GN-II | GN-III | MGTE |
|-----|------------|------------|------------|------------|------------|
| 1.0 | -0.784896 | -0.772477 | -0.775711 | -0.8500569 | -0.773825 |
| 1.1 | -0.1207522 | -0.0872191 | -0.0584293 | -0.150888 | -0.0117255 |
| 1.2 | -0.0594166 | -0.0235388 | -0.0323295 | -0.0448969 | -0.0271417 |
| 1.3 | -0.0463577 | -0.0204745 | -0.02741 | -0.0189182 | -0.023363 |
| 1.4 | -0.0363321 | -0.0178935 | -0.0233439 | -0.0404948 | -0.0202036 |
| 1.5 | -0.0285732 | -0.0157009 | -0.0199572 | -0.0034499 | -0.0175404 |
| 1.6 | -0.022538 | -0.0138248 | -0.0171181 | -0.0014872 | -0.0152799 |
| 1.7 | -0.0178235 | -0.0122096 | -0.014725 | -0.0006442 | -0.01335 |
| 1.8 | -0.0141272 | -0.0108116 | -0.0126982 | -0.0002801 | -0.011694 |
| 1.9 | -0.0112198 | -0.009596 | -0.0109746 | -0.0001222 | -0.0102667 |
| 2.0 | -0.0089266 | -0.0085348 | -0.0095037 | -5.347E-05 | -0.009032 |

In all the demonstrated figures and tables, too, the phenomenon of limited diffusion speeds was observed. Data show that, because of the applied thermal shock at the medium’s free stress boundary, all the presented models have notable differences near the medium boundary, and the variations decrease with distance.

In this last case, we will study the change in the behavior of different fields with the change in distance and time together, which is different from the previous cases, in which the study was conducted with the change in the radius of the spherical cavity only. Figures 9, 10, 11, 12 (3D plot) show a comparison with the R directions r of different distances ($1 \leq R \leq 2$) and time dimensionless ($0.1 \leq \tau \leq 0.2$), when the gradient coefficient is consistent $\xi = 2$, as compared to temperature Θ , displacement U , and thermal pressures τ_{rr} and $\tau_{\varphi\varphi}$. In addition, Figures 9, 10, 11, 12 are shown to indicate at different times the type of differences in field quantities in accordance with the MGTE model. It is clear that the thermophysical fields are affected by the respective time instance. In the non-homogeneous case, Fig. 9 indicates that the temperature difference when $\xi = 2$ is graded, with different values in the non-dimensional instantaneous time τ or with different values of the radius R .

It is observed that the temperature is very sensitive to changing time τ as it increases with increasing τ while decreasing with increasing distance R . The decrease in heat waves agrees with the physical aspects and underscores the importance of the proposed new model. Moreover, the increase with time is near the surface of the spherical cavity as a result of the influence of thermal shock. It is also expected that, with the passage of time, the temperature will decrease again with time, leading to the disappearance of the thermal shock effect. Figure 10 displays the behavior of the radial displacement U with different values of instantaneous time τ along with the radial direction R of the spherical cavity.

We notice that the displacement values increase with increasing time, while in the direction of the radius they increase until they reach their maximum values and then gradually decrease until they disappear. Figures 11 and 12 in the 3D show the variations and behavior of radial and ring thermal stresses τ_{rr} and $\tau_{\varphi\varphi}$ with the change in distance R and time τ . We notice from the presented figures that the effect of time on thermal stresses is very prominent. We also notice that the stresses τ_{rr} and $\tau_{\varphi\varphi}$ decrease over time.

7 Conclusions

The main objective of this paper is to present a new generalized mathematical model (MGTE) for the theory of coupling thermoelasticity based on the Moore–Gibson–Thomson equation, which includes relaxation time in the heat flux vector. With the values of

Fig. 9 The temperature Θ with time τ and distance R

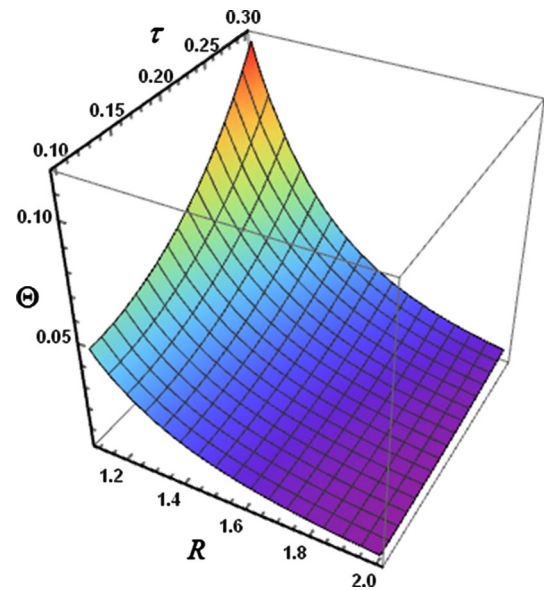
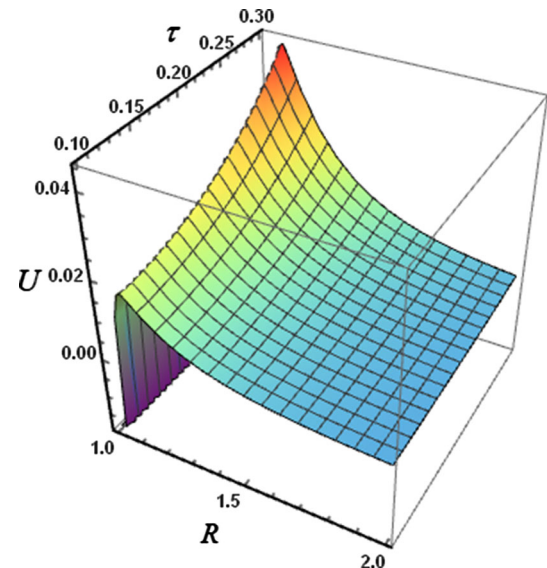


Fig. 10 The displacement U with time τ and distance R



the specified thermal parameters, the developed model is reduced to many theories in thermoelasticity. To the knowledge and belief of the author, the generalized MGTE thermoelastic model has not been found in very little published literature to date.

Analysis of thermal and mechanical waves and propagation behavior on an unbounded body with a spherical hole consisting of a functionally graded material in the radial variant has been studied as an application to this model. A graphical contrast of thermophysical fields was shown with a graded index of heterogeneous materials and compared with materials in a homogeneous state. In all tables and figures, the occurrence of finite propagation speeds has been confirmed. The thermal wave is expected to spread at a limited speed. This is expected. All the tables demonstrate that the MGTE model actually yields consistent results.

In the end, the impact of the non-homogeneous index literature on the field variables and the fractional order is very apparent. The findings provided in the article have been useful for materials scientists, designers of different materials, and investigators who are working to develop theories concerning the theory of elasticity and thermoelasticity.

Fig. 11 The radial stress τ_{rr} with time τ and distance R

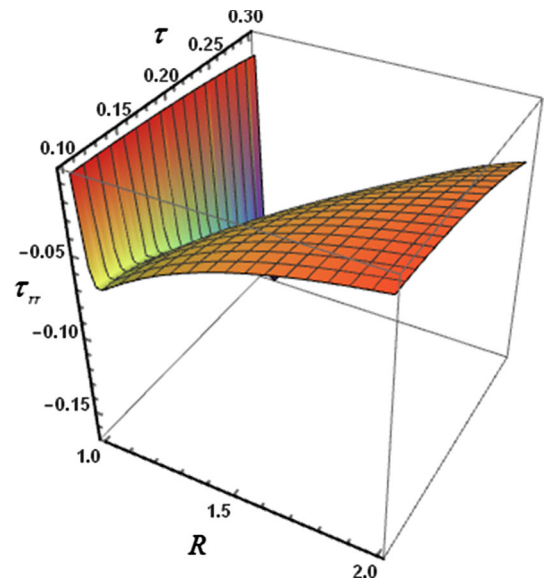
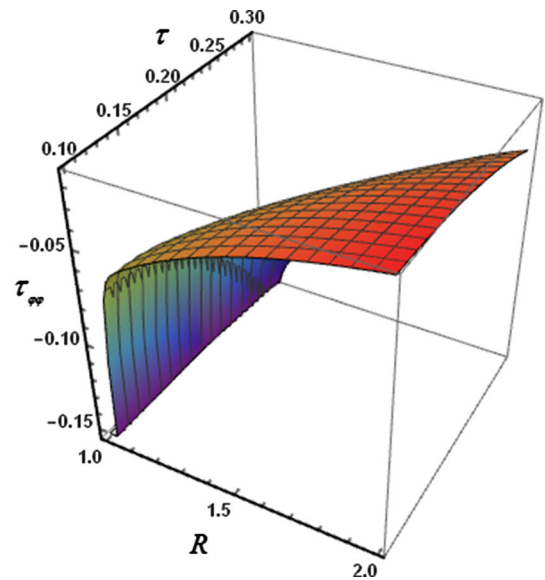


Fig. 12 The hoop stress $\tau_{\varphi\varphi}$ with time τ and distance R



Acknowledgements The authors extend their appreciation to the Deanship of Scientific Research at Jouf University for funding this work through research grant no. DSR-2021-03-0384.

Declarations

Conflict of interest The authors declare no conflict of interest.

References

1. M.H. Babaei, M. Abbasi, M.R. Eslami, Coupled thermoelasticity of functionally graded beams. *J. Therm. Stresses* **31**(8), 680–697 (2008)
2. M.K. Ghosh, M. Kanoria, Generalized thermoelastic functionally graded spherically isotropic solid containing a spherical cavity under thermal shock. *Appl. Math. Mech.* **29**(10), 1263–1278 (2008)
3. S. Banik, M. Kanoria, Generalized thermoelastic interaction in a functionally graded isotropic unbounded medium due to varying heat source with three-phase-lag effect. *Math. Mech. Solids* **18**(3), 231–245 (2012)
4. A.E. Abouelregal, H. Ahmad, S.-W. Yao, Functionally graded piezoelectric medium exposed to a movable heat flow based on a heat equation with a memory-dependent derivative. *Materials* **13**(18), 3953 (2020)
5. P.K. Karsh, R.R. Kumar, S. Dey, Stochastic impact responses analysis of functionally graded plates. *J. Braz. Soc. Mech. Sci. Eng.* **41**, 501 (2019)

6. S.M. Abo-Dahab, A.E. Abouelregal, M. Marin, Generalized thermoelastic functionally graded on a thin slim strip non-Gaussian laser beam. *Symmetry* **12**(7), 1094 (2020)
7. A.E. Abouelregal, S.-W. Yao, H. Ahmad, Analysis of a functionally graded thermopiezoelectric finite rod excited by a moving heat source. *Results Phys.* **19**, 103389 (2020)
8. W. Hasona, M. Adel, effect of initial stress on a thermoelastic functionally graded material with energy dissipation. *J. Appl. Math. Phys.* **8**, 2345–2355 (2020)
9. A.E. Abouelregal, E.D. Husam, Memory and dynamic response of a thermoelastic functionally graded nanobeams due to a periodic heat flux. *Mech. Based Design Struc. Mach.* (2021). <https://doi.org/10.1080/15397734.2021.1890616>
10. A.E. Abouelregal, Size-dependent thermoelastic initially stressed micro-beam due to a varying temperature in the light of the modified couple stress theory. *Appl. Math. Mech. Engl. Ed.* **41**, 1805–1820 (2020)
11. A.E. Abouelregal, W.W. Mohammed, H. Sedighi, M. Vibration analysis of functionally graded microbeam under initial stress via a generalized thermoelastic model with dual-phase lags. *Arch. Appl. Mech.* **91**, 2127–2142 (2021)
12. R.B. Hetnarski, M.R. Eslami, G.M.L. Gladwell, *Thermal Stresses: Advanced Theory and Applications Solid Mechanics and its Applications* (Springer, Heidelberg, 2010)
13. M.A. Biot, Thermoelasticity and irreversible thermodynamics. *J. Appl. Phys.* **27**(3), 240–253 (1956)
14. H.W. Lord, Y. Shulman, A generalized dynamical theory of thermoelasticity. *J. Mech. Phys. Solids* **15**(5), 299–309 (1967)
15. A.E. Green, K.A. Lindsay, Thermoelasticity. *J. Elast.* **2**(1–7), 7 (1972)
16. A.E. Green, P.M. Naghdi, A re-examination of the basic postulates of thermomechanics. *Proc. R. Soc. Lond.* **432**(1885), 171–194 (1991)
17. A.E. Green, P.M. Naghdi, On undamped heat waves in an elastic solid. *J. Therm. Stress.* **15**(2), 253–264 (1992)
18. A.E. Green, P.M. Naghdi, Thermoelasticity without energy dissipation. *J. Elast.* **31**(3), 189–208 (1993)
19. D.S. Chandrasekharaiyah, Hyperbolic thermoelasticity: a review of recent literature. *Appl. Mech. Rev.* **51**(12), 705–729 (1998)
20. D.Y. Tzou, The generalized lagging response in small-scale and high-rate heating. *Int. J. Heat Mass Transf.* **38**(17), 3231–3240 (1995)
21. S.K. RoyChoudhuri, On a thermoelastic three-phase-lag model. *J. Therm. Stresses* **30**(3), 231–238 (2007)
22. A.E. Abouelregal, Modified fractional thermoelasticity model with multi-relaxation times of higher order: application to spherical cavity exposed to a harmonic varying heat. *Waves Rand. Compl. Med.* **13**(5), 812–832 (2021)
23. A.E. Abouelregal, On Green and Naghdi thermoelasticity model without energy dissipation with higher order time differential and phase-lags. *J. Appl. Comput. Mech.* **6**(3), 445–456 (2020)
24. A.E. Abouelregal, Two-temperature thermoelastic model without energy dissipation including higher order time-derivatives and two phase-lags. *Mater. Res. Express* **6**, 116535 (2019)
25. A.E. Abouelregal, A novel model of nonlocal thermoelasticity with time derivatives of higher order. *Math. Meth. Appl. Sci.* **43**(11), 6746–6760 (2020)
26. R. Quintanilla, Moore-Gibson-Thompson thermoelasticity. *Math. Mech. Solids* **24**, 4020–4031 (2019)
27. R. Quintanilla, Moore-Gibson-Thompson thermoelasticity with two temperatures. *Appl. Engin. Sci.* **1**, 100006 (2020)
28. A.E. Abouelregal, I.-E. Ahmed, M.E. Nasr, K.M. Khalil, A. Zakria, F.A. Mohammed, Thermoelastic processes by a continuous heat source line in an infinite solid via Moore-Gibson-Thompson thermoelasticity. *Materials* **13**(19), 4463 (2020)
29. A.E. Abouelregal, H.M. Sedighi, The effect of variable properties and rotation in a visco-thermoelastic orthotropic annular cylinder under the Moore-Gibson-Thompson heat conduction model. *Proc. Inst. Mech. Eng. Part L J. Mater. Design Appl.* **235**(5), 1004–1020 (2021)
30. B. Kaltenbacher, I. Lasiacka, R. Marchand, Wellposedness and exponential decay rates for the Moore-Gibson-Thompson equation arising in high intensity ultrasound. *Control Cybernet.* **40**, 971–988 (2011)
31. M. Conti, V. Pata, R. Quintanilla, Thermoelasticity of Moore-Gibson-Thompson type with history dependence in the temperature. *Asympt. Anal.* **120**(1–2), 1–21 (2020)
32. M. Pellicer, R. Quintanilla, On uniqueness and instability for some thermomechanical problems involving the Moore-Gibson-Thompson equation. *Z. Angew. Math. Phys.* **71**, 84 (2020)
33. K. Jangid, S. Mukhopadhyay, A domain of influence theorem for a natural stress-heat-flux problem in the Moore-Gibson-Thompson thermoelasticity theory. *Acta Mech.* **232**, 177–187 (2021)
34. N. Bazarra, J.R. Fernandez, R. Quintanilla, Analysis of a Moore-Gibson-Thompson thermoelasticity problem. *J. Comput. Appl. Math.* **382**, 113058 (2021)
35. M. Conti, V. Pata, M. Pellicer, R. Quintanilla, On the analyticity of the MGT-viscoelastic plate with heat conduction. *J. Differ. Equ.* **269**(10), 7862–7880 (2020)
36. J.R. Fernández, R. Quintanilla, Moore-Gibson-Thompson theory for thermoelastic dielectrics. *Appl. Math. Mech.-Engl. Ed.* **42**, 309–316 (2021)
37. F. Dell’Oro, V. Pata, On the Moore-Gibson-Thompson equation and its relation to linear viscoelasticity. *Appl. Math. Optim.* **76**, 641–655 (2017)
38. A.E. Abouelregal, Generalized thermo-elasticity in an infinite nonhomogeneous solid having a spherical cavity using DPL model. *Appl. Math.* **2**(5), 625–632 (2011)
39. A.E. Abouelregal, Three-phase-lag thermoelastic heat conduction model with higher-order time-fractional derivatives. *Indian J. Phys.* **94**, 1949–1963 (2020)
40. G. Honig, U. Hirdes, A method for the numerical inversion of the Laplace transform. *J. Comput. Appl. Math.* **10**, 113–132 (1984)

Springer Nature or its licensor holds exclusive rights to this article under a publishing agreement with the author(s) or other rightsholder(s); author self-archiving of the accepted manuscript version of this article is solely governed by the terms of such publishing agreement and applicable law.